RESEARCH PAPER

Investigation of Structural and Optical Behaviors of Nanocomposite-Doped Polyethylene Oxide Films

Alhak A. M. Hassan *, Abdulazeez O. Mousa Al-ogaili

Department of Physics, College of Science, University of Babylon, Iraq

ARTICLE INFO

Article History:
Received 04 June 2025
Accepted 20 September 2025
Published 01 October 2025

Keywords:
Coffee husk
FESEM
Nanocomposite
Optical properties
Polyethylene oxide
XRD

ABSTRACT

The present study investigates how incorporating 5 wt.% coffee husk (CH) powder affects the structural and optical characteristics of composite films created from high-molecular-weight polyethylene oxide (PEO). The solution casting method was used to make the PEO-CH composite films. The XRD analysis showed that all of the produced films had a semicrystalline structure. The FTIR analysis confirmed the presence of multiple functional groups in the matrix of PEO. The observed absorption bands correspond to C–H stretching and bending vibrations, O–H groups, and a characteristic C–O–C triplet bond, indicative of the polymer's molecular structure. FESEM examination demonstrated that coffee husk particles exhibited plate-like morphology. The EDX elemental analysis of pure PEO films showed that they contained 54.6% carbon and 45.4% oxygen, while the doped films had additional elements: 55.2% carbon, 43.7% oxygen, 0.4% aluminum, 0.3% silicon, 0.1% potassium, 0.1% calcium, and 0.2% nickel. The optical properties of the PEO-based composite films, which were 97.5 μm and 83.5 μm thick, were studied using methods like measuring how much light passed through and how much was reflected and analyzing the refractive index and extinction coefficient. The UV-Vis absorption spectrum of pure PEO exhibited a single absorption peak at 240 nm. Incorporation of CH reduced both direct and indirect bandgap energies from 4.5 eV to 2.9 eV and from 3.3 eV to 1.5 eV, respectively.

How to cite this article
Hassan A., Al-ogaili A. Investigation of Structural and Optical Behaviors of Nanocomposite-Doped Polyethylene Oxide Films. J Nanostruct, 2025; 15(4):2479-2491. DOI: 10.22052/JNS.2025.04.084

INTRODUCTION

A growing research interest has emerged in response to the urgent global demand for waste reduction and the development of sustainable alternatives through the utilization of novel renewable resources. This approach shows the benefits of using different types of waste biomass as renewable, affordable, and easily accessible materials, providing a practical way to lower energy use and raw material costs [1]. In recent decades, significant efforts have been directed toward the development of sustainable and environmentally friendly products aimed at reducing reliance on fossil fuels. In addition to the rapid expansion of the renewable energy sector, particularly in photovoltaics, growing environmental concerns have intensified the urgency to eliminate petroleum-based plastics from ecosystems. Such an effort has catalyzed extensive research into biodegradable and bio-based polymers, commonly referred to as biopolymers. These materials are derived from natural and plant-based sources,

* *Corresponding Author Email: sci.elhaq.abd@uobabylon.edu.iq*

including agricultural residues, forestry biomass, horticultural waste, and various crop by-products. They are now finding their day-to-day applications, especially polymers that are biodegradable or based on renewable "feedstock," which may soon compete with commodity plastics [2]. Polyethylene oxide (PEO) is a semi-crystalline, water-soluble polymer with non-ionic and hydrophilic properties. This versatile material finds extensive applications in drug delivery systems, tissue engineering scaffolds, and biomedical device fabrication. For optimal performance in these applications, PEO must exhibit appropriate thermodynamic properties, controlled crystallization behavior, and sufficient molecular weight characteristics [3]. PEO films are widely researched as a type of polymer film because they are inexpensive, stable in chemical and electrical environments, durable during reduction processes, can easily dissolve metal ions, and have both solid- and liquid-like properties. These characteristics render PEO a viable material for various applications, including fuel cells, lithium-ion batteries, hybrid power supercapacitors, transistors, sensors, and memory technologies [4]. PEO shows no toxicity, antigenicity, or immunogenicity. The features of PEO render it a flexible polymer with diverse applications, including polymer electrolytes, biomedical purposes, pharmaceuticals, and more. Additional significant uses encompass batteries and cellular technologies [5]. The optical properties of polymers enhance understanding of their internal structure and the nature of their linkages, thereby expanding the scope of potential applications. To ascertain the various optical properties across different wavelength ranges, it is essential to study the absorption, reflectivity, and transmittance spectra of bonds, energy rays, and orbitals by analyzing the ultraviolet (UV) spectrum. Therefore, examining the visible spectrum yields adequate information about the material's behavior for many applications, including electro-optic and solar energy technologies. The electrical phenomenon can be characterized by the movement of charge units, referred to as charge carriers, which is influenced by the effect of potential difference. Polymers exhibit some conduction processes, and numerous charge carriers may demonstrate low-level conduction. The electrical conductivity of materials can be classified as insulators, semiconductors, conductors, and superconductors. The electrical properties of the material are influenced by both its chemical composition and the atomic arrangement inside the solid, as well as the presence of defects that contribute to the electron states in the energy gap. This defect can be reduced through various processes, like the annealing process. [6]. Coffee represents a significant commodity product that originates from coffee beans. Coffee ranks among the most widely consumed beverages globally, and its commercial importance has grown remarkably in the last century and a half based on data from the International Coffee Organization (ICO) [7]. The use of agricultural waste, such as coffee husks, provides a source of renewable material in construction and a non-food source of economic development for agriculture and rural areas in different countries [8]. Coffee husk is a high-density, eco-friendly material that is cost-effective and may potentially substitute produced fibers in various sectors. Coffee husk is crucial for the production of value-added products, although it is underutilized given the available resources [9]. Coffee husks are a plentiful and underexploited biomass byproduct of coffee production. Tests showed that coffee husks contain 39.2% cellulose, 12.6% hemicellulose, 23.3% Klason lignin, 2.9% acid-soluble lignin, 8.7% extractives, and 9.5% ash. Additionally, researchers identified several trace elements, including K, Ca, Mg, Al, Fe, Ti, S, and Si [10]. Coffee husk flour is used in food production, biomedicine, and plastic wood in household items, automobile interior parts, and telephone closing boxes [11, 12, 13]. A 2023 study by AL-Akhras and others looked at the light and chemical properties of thin films made from a mix of polyethylene oxide (PEO) and curcumin nanoparticles. The study found that the refractive index values from UV-Vis spectroscopy were between 1.5 and 2.0 for the samples. Pure PEO films had an energy gap of 4.16 eV, curcumin nanoparticles had a lower energy gap of 2.49 eV, and the mix of PEO and curcumin kept the same energy gap of 4.16 eV as the pure PEO. Additionally, the study found that as the film got thinner, it absorbed light better, showing that there is a reverse connection between how thick the film is and how well it absorbs light [14]. In 2024, Abdali and others demonstrated the use of Elettaria cardamomum husk ash as a filler to enhance PEO polymer composites. Their study found that the composites had improved features in several areas, such as structure, light behavior, and electrical performance, which makes them

suitable for use in optoelectronic devices. The optical tests showed a big drop in both direct and indirect bandgap energies after adding the husk ash nanofibers; the direct bandgap went down from 5.85 eV to 2.85 eV, and the indirect bandgap fell from 3.85 eV to 2.25 eV [15].

The major objective of this research is to examine how nanofibers made from coffee husk ash affect the structural and optical characteristics of PEO polymer, rendering it suitable for diverse applications in optical electronics, protection from ultraviolet rays, food packaging, biomedicine, household items, telephone enclosures, and automotive plastic wood material technology.

MATERIALS AND METHODS

Materials

The polymer used in this study is PEO, a white granular material with high water solubility. It has a molecular weight of 3×10^6 g/mol and a purity of 98%. Chengdu ICXY Chemical Co., Ltd. supplies the PEO. Coffee husk and another material used in this study are obtained from an Iraqi local store.

Preparation of Coffee Husk (CH) Nanofibers

The coffee husk (CH) was prepared by collecting and thoroughly cleaning coffee plant husks to eliminate dust and impurities, as they were intended solely for use as a filler material. The cleaned husks were turned into a fine powder using a universal mill made of stainless steel, which ran at 50–60 Hz, 25,000 rpm, and 650 W, and could make the powder as fine as 30–300 mesh. The grinding process was conducted intermittently over a total duration of 60 minutes. Subsequently, the ground CH nanofibers of 0.05 g was obtained and employed as an eco-friendly filler throughout this study.

Preparation of PEO and PEO-CH Nanocomposite Films

At first, 1 gram of PEO was mixed into deionized water (H_2O) while being stirred continuously with a Stuart magnetic stirrer at room temperature (RT) (20 ± 5 °C) for 1 hour to create a homogeneous solution. After that, a 5 cm plastic Petri dish was utilized to contain the polymer solution. while it dried for 10 days under a chemical fume hood at RT to prevent contamination by dust, yielding a pristine PEO film. To create the nanocomposite, 5% coffee husk (CH) nanofibers were added to the PEO solution, and then it was stirred with a magnet for 35 minutes to ensure everything was mixed well, followed by the same casting and drying steps used for the pure PEO film. The thickness of the PEO-CH nanocomposite films was measured using a digital micrometer, revealing values between 97.5 and 83.5 micrometers. The specimens are designated as (PEO with 5 wt.% CH nanofibers).

Materials Characterization Methods

The coffee husk was ground utilizing a powder grinder (provided by Chengdu Micxy Chemical Co., Ltd.). Structural examination was performed employing XRD (X-ray diffraction) on an Aeris diffractometer (Malvern Panalytical) with Cu-Kα radiation (λ = 1.54 Å), functioning at 40 kV and 30 mA. The scan was performed within the 2θ range of 10° to 80°, utilizing a step size of 0.05° and a counting duration of 1.0 second per step. Fourier-transform infrared (FTIR) spectroscopy was carried out using a Vertex 70 spectrometer (Bruker, Germany) to analyze functional groups. Morphological and elemental composition analyses were conducted using field-emission scanning electron microscopy (FESEM) and energy-dispersive X-ray spectroscopy (EDX) with an INSPECT F50 FE-SEM. The optical properties were checked using a Shimadzu UV-Vis spectrometer.

RESULTS AND DISCUSSION

XRD analysis

Fig. 1 presents the XRD patterns of pure PEO and the PEO-CH nanocomposite. The spectrum of pure PEO shows typical semicrystalline behavior, with two strong peaks at 19.4° and 23.5° (2θ), which indicate its crystalline structure, as shown in Fig. 1a. Additionally, smaller peaks appear at higher angles of 27.10°, 36.39°, and 39.89°, further supporting the concept that the polymer contains both crystalline and non-crystalline regions. The diffraction peaks observed at 19.4°, 23.5°, and 27.1° correspond to the (112), (120), and (121) crystal structures of PEO, as indicated by standard reference patterns. The broadening of these peaks in the PEO diffraction pattern suggests that the polymer exhibits a linear semicrystalline structure. This structural characteristic is crucial for stabilizing PEO both chemically and electrochemically. The crystallization process in such polymers typically occurs through hierarchical organization across multiple length scales. During this process, the bending of polymer chains results in the formation

of unique folded-chain layers that exhibit a specific molecular pattern. This chain-folding arrangement permits unconstrained expansion in two lateral dimensions. However, there is a limitation on the propagation of chain extension, with most defects concentrated at the folding surfaces. The peaks seen in Fig. 1 are caused by strong interactions between PEO chains that are linked by hydrogen bonds, along with the arrangement of the polyether side chains. This finding is consistent with previous studies referenced in [16, 17, 15], which indicated that the crystalline peaks for a pure PEO sample appeared at these specific angles. The different shapes of the diffraction peaks illustrate the crystalline or semicrystalline nature of the PEO polymer surfaces [17]. The XRD pattern for the PEO-CH nanocomposite is shown in Fig. 1b. The XRD patterns show that the composite material has some crystalline structure, as seen by two strong peaks at 19.3° and 23.6°, which are common for the polyethylene oxide (PEO) polymer. Additionally, the composite spectrum reveals several low-intensity reflections at 2θ values of 26.3°, 27.1°, 36.3°, and 39.8°. The changes seen in the XRD pattern indicate that adding filler material affects the crystal structure of PEO, which might change how the chains are arranged and the size of the crystals. The peak broadening effect shows that either the crystallite size has decreased or the polymer structure is more disordered when the composite is made. In summary, the XRD results show that adding more coffee husk (CH)

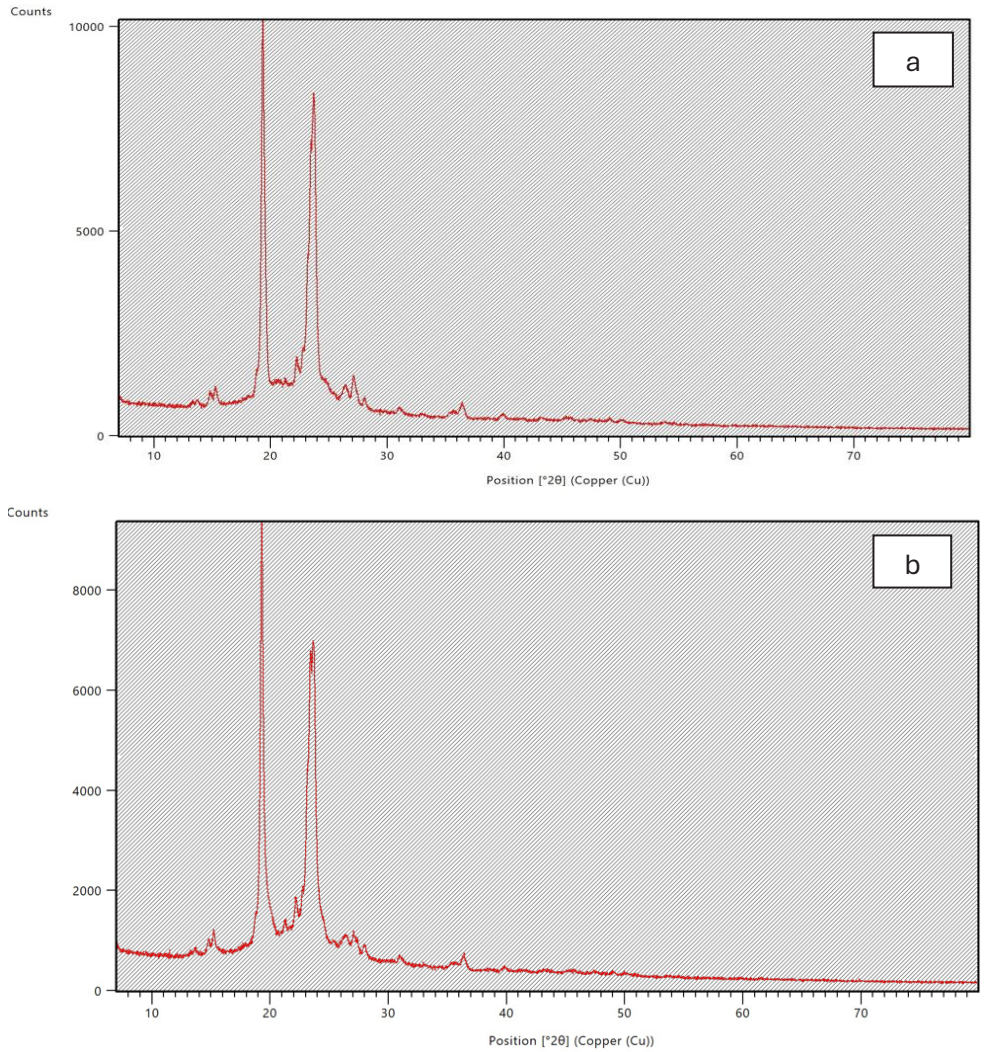

Fig. 1. XRD analyses of (a) PEO and (b) PEO-CH.

nanofibers to the PEO matrix causes the peaks in the diffraction pattern to spread out more. This phenomenon can be attributed to structural modifications within the polymer matrix, which may stem from changes in the degree of crystallinity of PEO, shifts in polymer chain packing due to the incorporation of nanofibers, and potential interactions between the PEO and CH components. The size of the crystallites (D) was determined using the Debye-Scherrer equation, which correlates the broadening of the peaks to the size of the crystalline regions, as represented in Equation (1) [15].

$$D = K\lambda/\beta cos\theta \quad (1)$$

where k represents the shape factor (0.9 for spherical crystals), β denotes the full width at

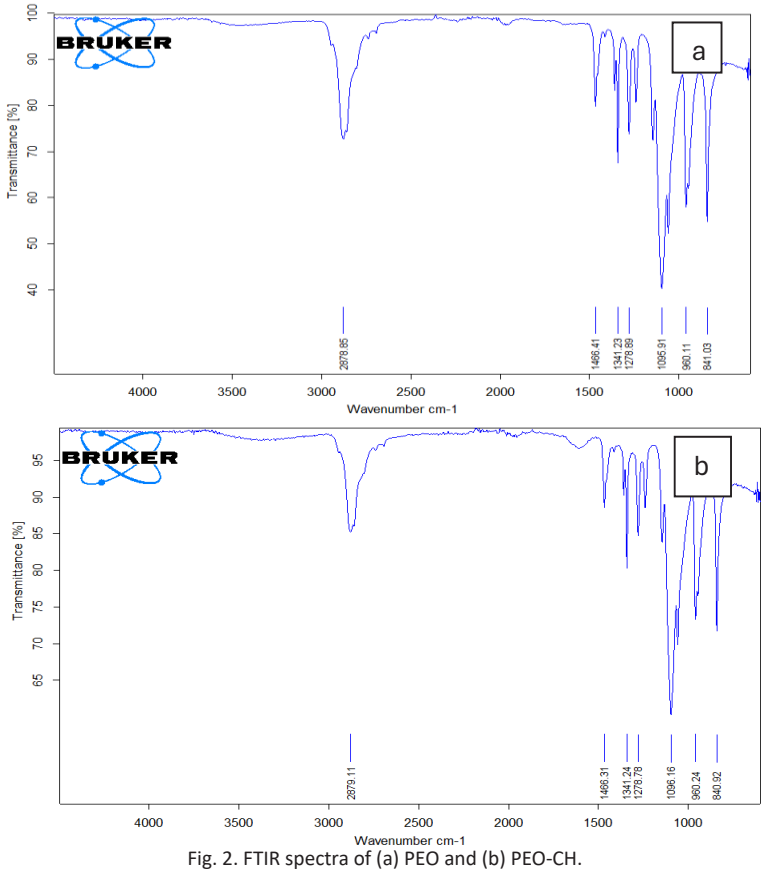

Fig. 2. FTIR spectra of (a) PEO and (b) PEO-CH.

Table 1. the band allocations for the FTIR analysis of PEO and PEO-CH [20-23].

Absorption(cm^{-1})	Appearance	Group	Compound Class
2878	medium	C-H stretching	alkane
1466	medium	C-H bending	alkane
1341	medium	C-H bending	alkane
1278	strong	C-O stretching	Alkyl aryl ether
1095	strong	C-O stretching	Secondary alcohol
960	strong	C=C bending	alkene
841	medium	C=C bending	alkene

half maximum (FWHM) of the diffraction peak (in radians), and θ is the Bragg diffraction angle. The analysis shows that as the crystallite size gets smaller, (cos θ) $^{-1}$ gets larger, and lattice strain increases with tan θ. These relationships demonstrate how peak broadening effects correlate with both finite crystallite dimensions and structural distortions within the material. The crystallite size corresponding to the most intense peak in PEO polymer is 31 nm, while after the addition of coffee husks, it decreases to 27.5 nm. Due to Coffee husks contain fibrous materials such as cellulose, which can act as nucleation sites to enhance crystallization in certain polymers. However, in some cases, this addition may lead to a reduction in the degree of crystallinity due to the interference of the fibers with the alignment of polymer chains. The peak intensities significantly diminished, resulting in a change in the crystalline size of the PEO polymer, with a reduction in the crystallite size of PEO upon the incorporation of CH nanofibers [18,19]. The nanocomposite films' XRD patterns do not show any new peaks.

Fourier-Transform Infrared (FTIR) Spectroscopy Analysis

FTIR spectroscopy was utilized to characterize the functional groups present in both pure PEO and PEO/CH nanocomposite films. Spectra were recorded across the mid-infrared range (400–4000 cm^{-1}), which enables comprehensive identification of molecular vibrations associated with organic functional groups (PEO polymer matrix) and potential inorganic components (from CH Nano fillers) [17]. The FTIR spectra of PEO and PEO-CH are shown in Fig. 2. The stretching vibrations of C-H bonds were shown by a spectral band at 2883 cm−1 in the PEO spectrum, whereas the bending vibrations of C-H bonds were indicated by bands at 1467 and 1341 cm^{-1}. The bands of absorption seen from 1280 to 1100 cm^{-1} are due to the stretching movements of the O-H and C-O-C ether bonds. The triplet at 1095 cm^{-1} represents the symmetrical stretching of the C-O-C group, confirming the existence of a crystalline phase in PEO [20, 21, 22]. The C-O-C and CH rocking vibrational modes occur at 960 cm and 841 cm, respectively [22]. The band detected at 841 cm^{-1} corresponds to the stretching vibration of the molecular bonds C-O-C and C-C [23]. These results reveal a significant level of crystallinity within the PEO structure [24]. The FTIR spectra of PEO-CH are displayed in Fig. 2b. No additional absorption bands are detected compared to pure PEO. The main PEO peaks show up at slightly different wavenumbers, and these shifts suggest physical interactions rather than chemical ones, which is expected due to intermolecular forces. Table 1 displays the band allocations for the FTIR analysis of PEO and PEO-CH.

Morphological Characterization using (FESEM)

The morphological analysis was carried out using Field Emission Scanning Electron Microscopy (FESEM), a high-resolution imaging technique that produces a highly concentrated electron beam using a field emission electron source. This allows for the detailed visualization of surface structures with high clarity and depth [25]. FESEM is particularly valuable in fields such as nanotechnology and materials science, where accurate surface characterization and analysis at the nanoscale are essential [26]. Fig. 3 illustrates the results of the extensive investigation of the surface morphologies of the PEO and P-CH films. The FESEM micrograph of pure PEO reveals a rough surface morphology interspersed with smoother regions, as illustrated in Fig. 3a, which can be attributed to its semi-crystalline structure. In contrast, Fig. 3b shows that the incorporation of coffee husk nanoparticles did not result in any noticeable aggregation or cracking within the film. Plate-like structures were observed, likely originating from the presence of the coffee husk nanoparticles, which may have contributed to the formation of bimetallic nanoparticle structures. Furthermore, the coffee husk particles appeared to be uniformly and finely dispersed throughout the PEO matrix, likely due to the polymer's compatibility and ability to effectively incorporate nanocomposite particles [27]. The imaging results showed that the particle was 53.26 nm in size, according to Energy Dispersive X-ray Spectroscopy (EDX), a method used to study materials and find out their chemical properties. This approach indicated that the polymer comprised both oxygen and carbon. Fig. 3c shows the elemental analysis of the PEO film, which revealed the presence of carbon and oxygen at concentrations of 54.6% and 45.4%, respectively. Fig. 3d shows the EDX analysis of the PEO-CH films, which contain the elements C, O, Al, Si, K, Ca, and Ni in the following amounts: 55.2%, 43.7%, 0.4%, 0.3%, 0.1%, 0.1%, and 0.2%. The data indicate that the high-intensity element

is carbon, which can be attributed to the polymer composition.

Optical Characterization by UV-Vis Spectroscopy

A spectrophotometer recorded the UV-Vis spectrum within the optical range of 190 to 1100 nm. UV-Vis spectroscopy measures the attenuation of a light beam after it passes through or is reflected from a sample. Fig. 4 presents the absorption spectra of both pure

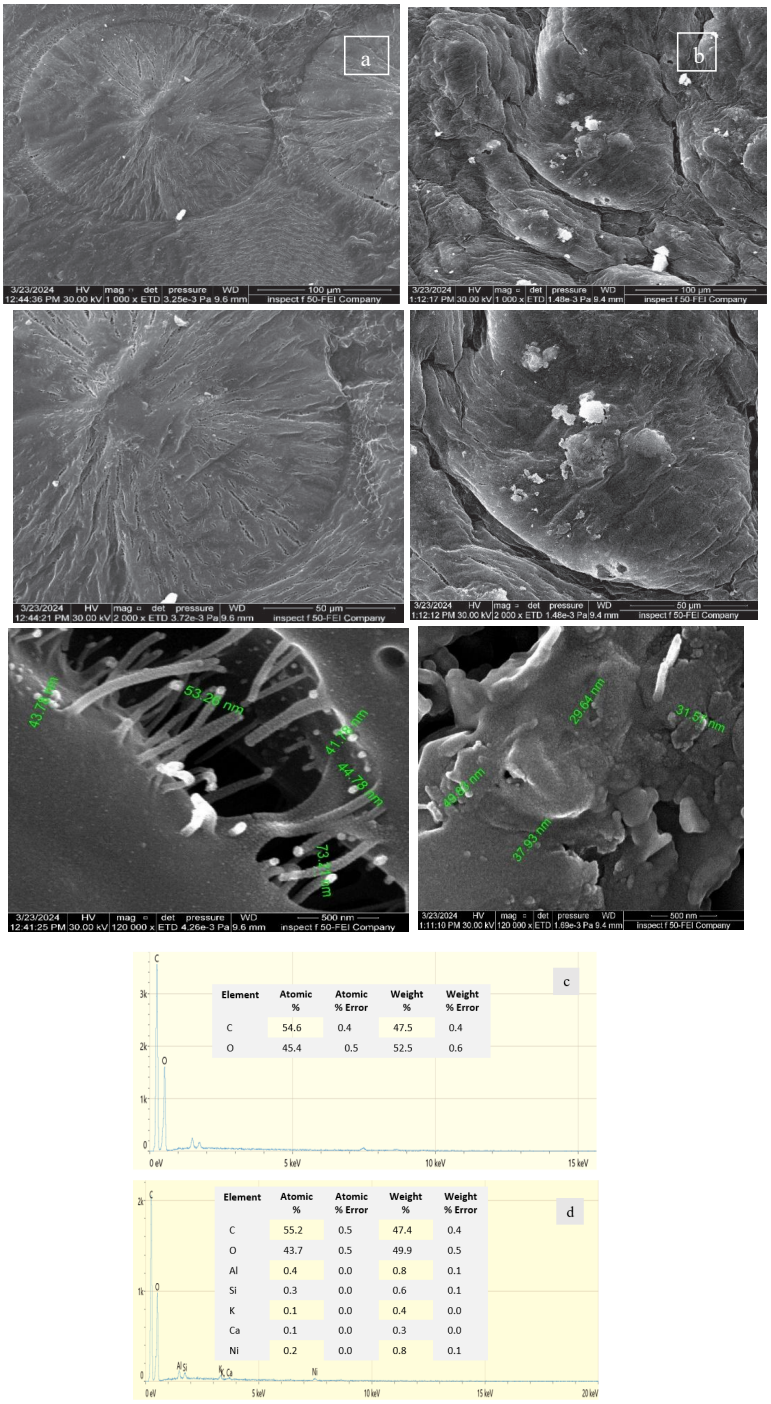

Fig. 3. FESEM-EDX of (a) PEO and (b) PEO-CH, EDX of (c) PEO and (d) PEO-CH.

PEO and the PEO-CH nanocomposite. The pure PEO spectrum has a noticeable absorption peak around 240 nm, probably due to n→π* electronic transitions (R-band). These transitions are generally linked to non-bonding electrons in single bonds, indicating absorption primarily in the far-ultraviolet region. Upon incorporation of coffee husk (CH) nanoparticles into the PEO matrix, a substantial rise in absorbance across the UV-Vis range is observed. This is evidenced by an elevated absorption coefficient and a noticeable red shift in the absorption edge, suggesting a transition toward longer wavelengths. This red shift is indicative of complexation between the coffee husk components and the polymer matrix and also reflects modifications in the optical band gap. These changes are likely related to alterations in the degree of crystallinity within the PEO structure [28]. the maximum absorption of PEO-CH film shifts to a longer wavelength at the absorption edge and exhibits a smaller band gap, this finding shows that there are CH nanofiber grains of different shapes and sizes spread out over the surface of the film, as shown by the FESEM examination [15]. Transmittance and reflectance spectra, as shown in Fig. 5, were used to analyze the optical properties. A transmittance value of less than 460 nm was observed for both

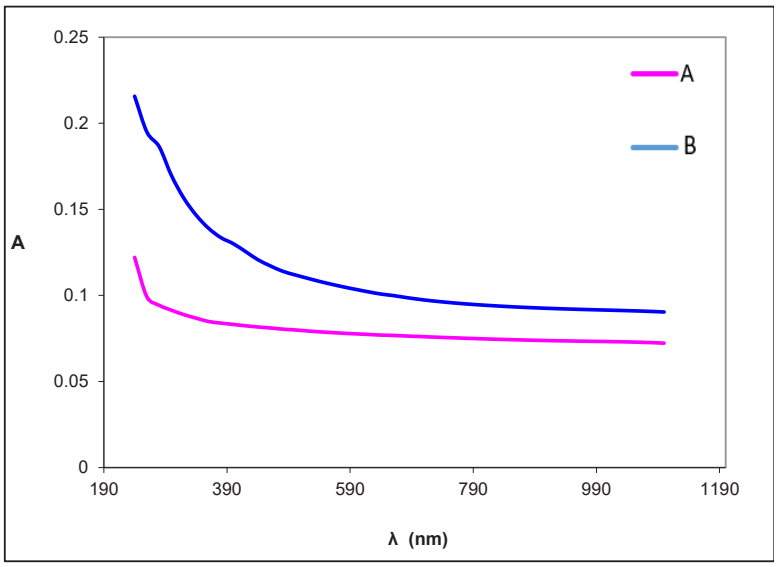

Fig. 4. Absorbance spectrum of PEO (A) and PEO-CH (B).

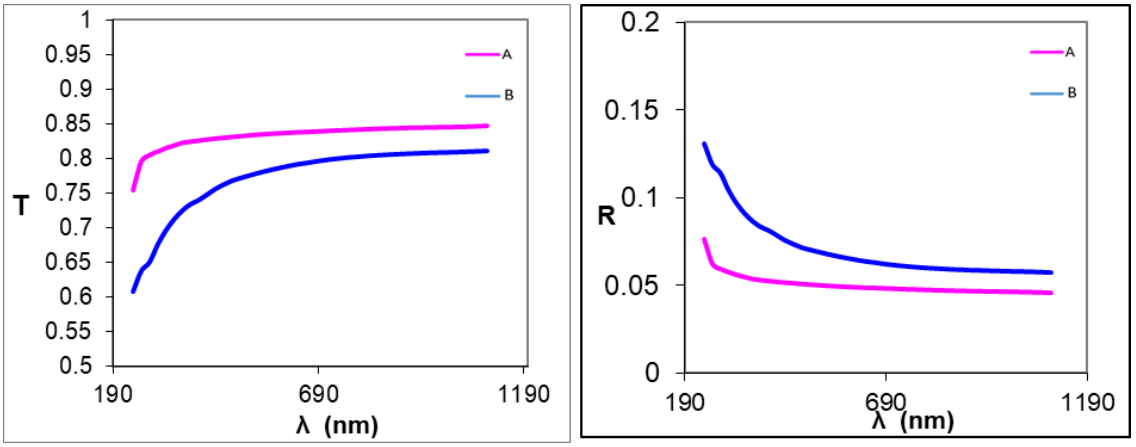

Fig.5. Transmittance and reflectance spectra of PEO (A) and PEO-CH (B).

PEO and PEO-CH. However, a cut-off wavelength of less than 360 nm was observed in the pure PEO membrane [14]. Transmittance curves for all samples show a saturation tendency; in the visible and near-infrared bands, the polymer films reach an average maximum of about 50%. Nevertheless, transmittance decreases with an increase in the concentration of CH nanofibers within the PEO matrix. This behavior is mostly ascribed to alterations in film morphology and enhanced light absorbance. The reduced UV transmittance of the PEO-CH film renders it especially appropriate for applications including solar energy collectors, ultraviolet protection, and pharmacy packaging. [15].

The absorption coefficient is an important optical parameter derived from transmittance and reflectance data. It is a useful tool for evaluating the optical bandgap of nanocomposite films. Fig. 6 shows how the absorption coefficient changes with wavelength for both pure PEO and PEO-CH nanocomposite films. This coefficient reflects the probability that the material will absorb photons in relation to the unit length. It is notably influenced by the film's thickness, typically increasing as the thickness decreases. Thus, analyzing the absorption coefficient provides important information regarding the optical and structural characteristics of the films.

The absorption coefficient (A) is frequently computed using the relationship specified in Eq. 2 [12]. It serves as a sensitive physical parameter, providing essential information about the characteristics of charge carrier transitions and helping to determine the optical bandgap energy [29,30].

$$A = 2.303(a/t) \quad (2)$$

The absorbance is denoted by "a," and "t" represents the thickness of the film. The absorption coefficient is crucial for determining the type of electronic transition. Typically, absorption coefficient values below 10^4 cm^{-1} suggest an indirect electronic transition, whereas values exceeding 10^4 cm^{-1} indicate a direct transition.

The optical bandgap energy relates to the photon energy (hv) and the absorption coefficient according to the Tauc relation, as shown in Eq. 3.

$$Ah\upsilon = B\,(hv - E_g^{opt}) \pm Eph)^n \quad (3)$$

Where B denotes a constant related to the degree of structural disorder (band tailing), and n is an exponent that indicates the type of electronic transitions, with n = 0.5 representing indirect transitions and n = 2 denoting direct transitions. Plotting (αhv)1/n against photon energy (hv) yields the values of the direct and indirect optical bandgap energies, shown in Fig. 7. The optical bandgap was determined by extrapolating the linear region of the absorption curve to the photon

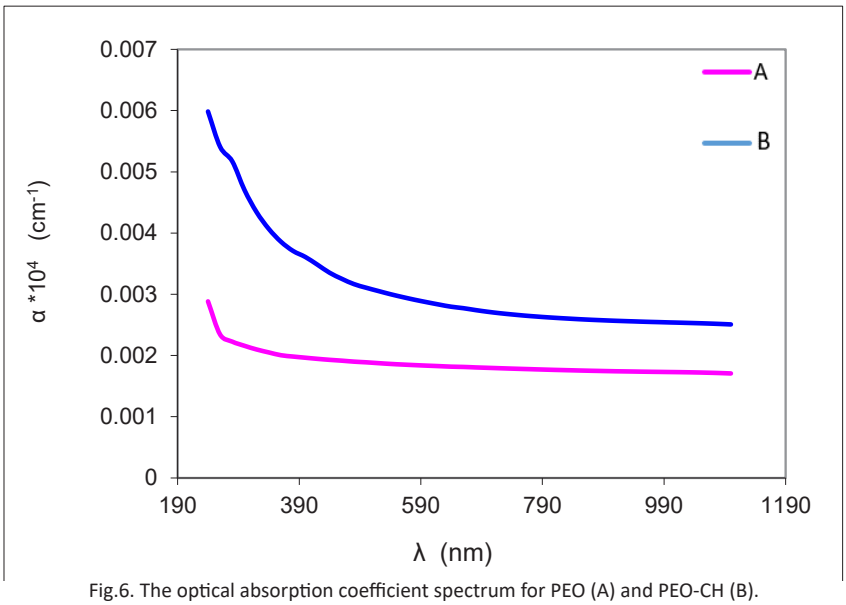

Fig.6. The optical absorption coefficient spectrum for PEO (A) and PEO-CH (B).

energy (hv) axis. The decrease in the bandgap as the additive concentration increases is due to the creation of structural defects and disorder close to the conduction band, which results in energy levels that are not evenly distributed within the bandgap. These states arise from interactions between the PEO matrix and CH nanofibers, enabling absorption of lower-energy photons. The indirect bandgap was found to be smaller than the direct bandgap. The direct bandgap of pure PEO decreased from 4.5 eV to 2.9 eV in the PEO-CH composite, but the indirect bandgap decreased from 3.3 eV to 1.5 eV. The decrease suggests that electronic transitions between the valence band maximum and conduction band minimum in the PEO-CH composite occur predominantly through indirect transitions. These findings are consistent with the literature [14, 15, 30].

Understanding the refractive index is crucial for analyzing various optical phenomena, as it is closely linked to ionic polarization and the internal electric field of optical materials. This variable is crucial for the advancement of systems with integrated optical components. The advancement of innovative substances in the optics and optoelectronic industries significantly depends on the optical dielectric constant. The refractive index can be calculated from a material's reflectance and absorption under electromagnetic radiation by using Eq. 4.

$$n * (\lambda) = n(\lambda) + ik(\lambda) \quad (4)$$

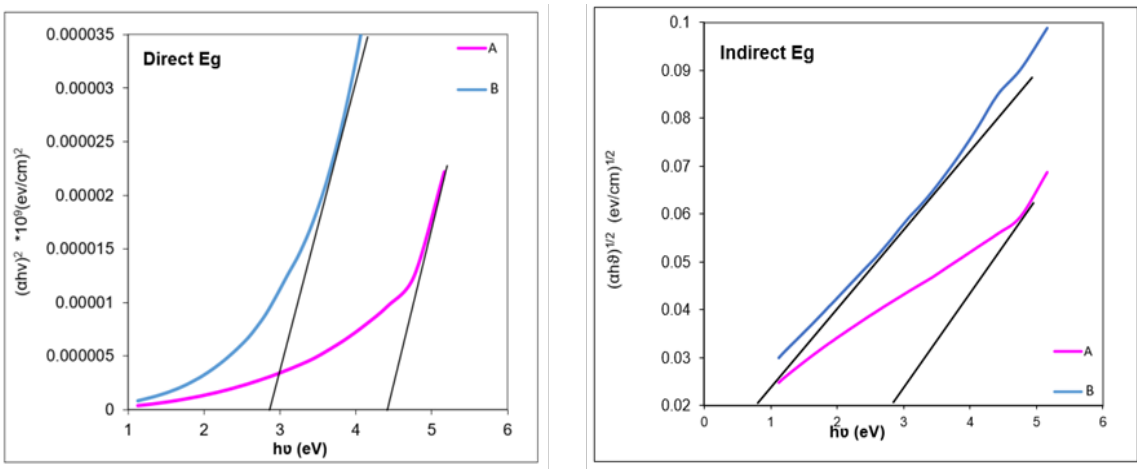

Fig. 7. Tauc diagram for PEO (A) and PEO-CH (B).

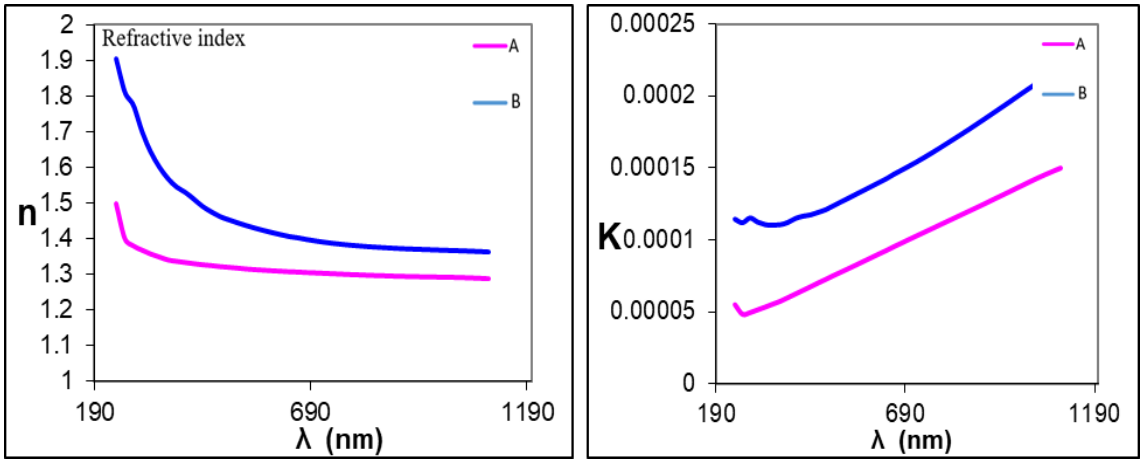

Fig. 8. Refractive index and Extinction coefficient spectra for PEO (A) and PEO-CH (B).

n*= complex refractive index, *n* = real part (related to the phase velocity of light), *k* = extinction coefficient (related to light absorption). The extinction coefficient (k) is commonly calculated using the absorption coefficient (α) and wavelength (λ):

$$k = \alpha \lambda / 4\pi \quad (5)$$

Furthermore, by using reflectance (R) and the extinction coefficient, the Fresnel equation can be calculated for the refractive indices of pure PEO and PEO-CH films. The analysis offers insights into the optical properties of these materials, which are essential for their application in photonic and optoelectronic devices.

The refractive index n(λ) was calculated using Equation 6, which relates the reflectance (R) and extinction coefficient (K):

$$n(\lambda) = \sqrt{\frac{4R}{(1-R)2} - K^2} + \frac{1+R}{1-R} \quad (6)$$

The refractive index serves as a critical indicator of material transparency, where values approaching zero suggest high transparency, whereas positive values indicate the absorption of light. The refractive index increased from 1.28 to 1.36 as a result of the incorporation of CH into PEO polymer, as demonstrated in Fig. 8. The formation of space charges in the CH is likely contributing to this rise [17]. A clear trend toward decreasing refractive index with increasing wavelength was observed throughout the visible spectrum [10], while the enhanced refractive index values broaden the material's potential for optoelectronic applications. The extinction coefficient that changes with wavelength for both pure PEO and PEO-CH nanocomposite films is displayed in Fig. 8. The nanocomposites showed increased extinction coefficients in the UV region, corresponding to strong absorption bands. This trend continued into the visible and near-infrared spectral regions, indicating enhanced light-matter interactions in the modified material system.

The dielectric constant consists of real (ε_r) and imaginary (ε_i) components that characterize distinct optical properties [31]. The real component ($\varepsilon_r = n^2 - k^2$) measures how much light slows down in the material, while the imaginary component ($\varepsilon_i = 2nk$) shows how energy is lost due to dipole interactions when an electric field is applied [32,33].

Fig. 9 illustrates the wavelength dependence of the real (ε_r) and imaginary (ε_i) components of the dielectric constant for CH and PEO-CH nanocomposites. The trend of the real component follows that of the refractive index (n), as the term k^2 becomes negligible in comparison to n^2. The imaginary component is directly proportional to the extinction coefficient (k) [34]. The observed increase in the dielectric constant of PEO-CH nanocomposites is attributed to reduced photon scattering. The higher ε_i values correspond to enhanced absorption coefficients, suggesting improved dipole alignment within the nanocomposite structure [30, 35, 36].

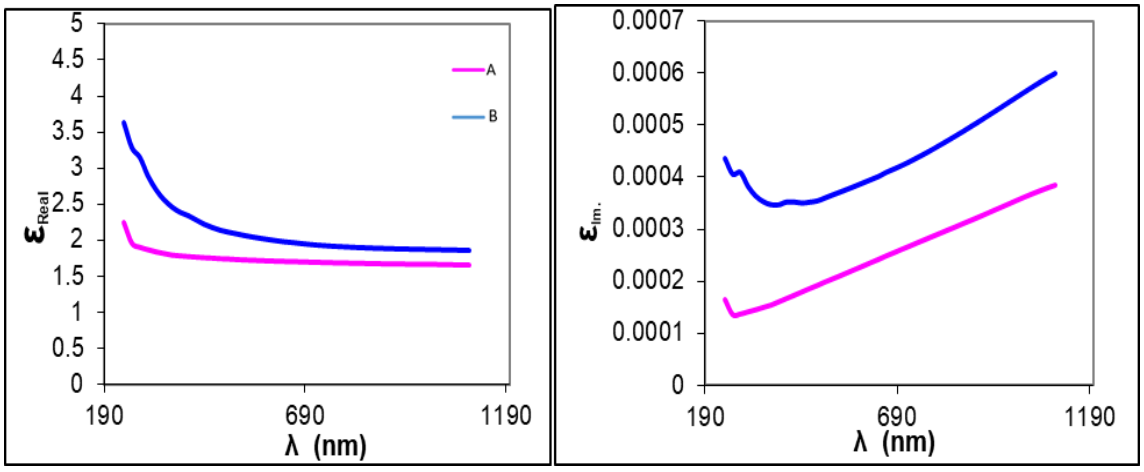

Fig. 9. Real and imaginary dielectric constant spectra for PEO (A) and PEO-CH (B).

CONCLUSION

In conclusion, the casting technique was employed to successfully synthesize PEO-CH nanocomposite films for the first time. XRD analysis of the composites revealed two main peaks at 19.4° and 23.5°, indicating that the polymer has a semicrystalline structure. The primary diffraction peaks of the nanocomposite films showed a decrease in intensity along with an increase in broadening, the diffraction peaks of the PEO matrix got broader when more CH nanofibers were added, which suggests that adding the nanofibers made the PEO crystals smaller. The XRD data showed no further diffraction peaks, suggesting the absence of new crystalline phases. FTIR analysis revealed conjugated double bonds and functional groups in PEO. These include C–H and O–H bond stretching and bending vibrations and C–O–C triplet bands. Although the PEO-CH nanocomposites' FTIR spectra exhibited no new peaks, the existing bands shifted compared with pure PEO, indicating physical interactions between the polymer matrix and the CH nanofibers. The images obtained from the FESEM of the PEO film demonstrated a surface that was homogeneous and smooth, free from defects, aggregation, or cracks. The coffee husk particles were finely and uniformly dispersed throughout the PEO matrix, likely due to the polymer's strong compatibility and effective integration with the nanocomposite particles. EDX analysis of the pure PEO film indicated carbon and oxygen contents at concentrations of 54.6% and 45.4%, respectively. After the doping process, additional elements such as Al, Si, K, Ca, and Ni were detected alongside C and O, with their respective weights being 55.2%, 43.7%, 0.4%, 0.3%, 0.1%, 0.1%, and 0.2%. The high-intensity component, attributed to the polymeric structure, is identified as C. The incorporation of coffee husks improved the optical properties. In the pure PEO film, an absorption peak was noted at approximately 240 nm, probably resulting from $n \rightarrow \pi^*$ transformations (R-band) involving single bonds, indicating that absorption predominantly occurs in the far UV region. By integrating CH into the PEO matrix, the absorbance in the UV/Vis region significantly increased. Furthermore, the PEO-CH film demonstrated the ability to absorb light at longer wavelengths, suggesting a smaller band gap and indicating that the CH nanofibers vary in size and shape on the surface film. The optical properties were examined by utilizing reflectance and transmittance spectra to evaluate key variables relevant to optoelectronic applications. Transmittance cut-offs below 360 nm were observed in the PEO film, but PEO-CH composites and pure PEO displayed similar cut-offs below 460 nm. The low UV transmittance of PEO makes it suitable for uses including solar collectors, UV protection, and packaging for pharmaceuticals. The direct transition energy decreased from 4.5 eV for pure PEO to 2.9 eV for PEO-CH, and the indirect transition energy decreased from 3.3 eV to 1.5 eV, respectively. The incorporation of coffee husks also increased the refractive index from 1.28 to approximately 1.36, enhancing the material's potential in optoelectronic devices.

CONFLICT OF INTEREST

The authors declare that there is no conflict of interests regarding the publication of this manuscript.

REFERENCES

1. Molahalli V, Sharma A, Bijapur K, Soman G, Chattham N, Hegde G. Low-cost bio-waste carbon nanocomposites for sustainable electrochemical devices: A systematic review. Materials Today Communications. 2024;38:108034.
2. Kakoria A, Sinha-Ray S. A Review on Biopolymer-Based Fibers via Electrospinning and Solution Blowing and Their Applications. Fibers. 2018;6(3):45.
3. Dalton M, Ebrahimi F, Xu H, Gong K, Fehrenbach G, Fuenmayor E, et al. The Influence of the Molecular Weight of Poly(Ethylene Oxide) on the Hydrolytic Degradation and Physical Properties of Polycaprolactone Binary Blends. Macromol. 2023;3(3):431-450.
4. Telfah AD, Abdalla S, Ferjani H, Tavares CJ, Etzkorn J. Optical, electrical, and structural properties of polyethylene oxide/fullerene nanocomposite films. Physica B: Condensed Matter. 2024;679:415787.
5. Al-Jamal AN, O KA, Abbass KH, Rabee BH, Al-Bermany E. Silver NPs reinforced the structural and mechanical properties of PVA-PAAm-PEG nanocomposites. AIP Conference Proceedings: AIP Publishing; 2023.
6. Al-Bermany E, Mekhalif ATm, Banimuslem HA, Abdali K, Sabri MM. Effect of green synthesis bimetallic Ag@SiO_2 core–shell nanoparticles on absorption behavior and electrical properties of PVA-PEO nanocomposites for optoelectronic applications. Silicon. 2023;15(9):4095-4107.
7. Melyna E, Afridana AP. The Effect of Coffee Husk Waste Addition with Alkalisation Treatment on the Mechanical Properties of Polypropylene Composites. Equilibrium Journal of Chemical Engineering. 2023;7(1):14.
8. Jaramillo HY, Vasco-Echeverri O, Camperos JAG. Characterization of the Coffee Husk: A Potential Alternative for Sustainable Construction. Civil Engineering and Architecture. 2023;11(4):1902-1908.
9. Amena BT, Altenbach H, Tibba GS, Hossain N. Physico-Chemical Characterization of Alkali-Treated Ethiopian Arabica Coffee Husk Fiber for Composite Materials

Production. Journal of Composites Science. 2022;6(8):233.
10. Nguyen DV, Duong CTT, Vu CNM, Nguyen HM, Pham TT, Tran-Thuy T-M, et al. Data on chemical composition of coffee husks and lignin microparticles as their extracted product. Data in Brief. 2023;51:109781.
11. Rebolledo Hernández MV, Cocotle-Ronzón Y, Hernández Martínez E, Morales Zarate E, Acosta Domíngez L. Propiedades fisicoquímicas, funcionales y de flujo de una harina de cáscara de café. CIENCIA ergo-sum. 2022;30(3).
12. Sisti L, Celli A, Totaro G, Cinelli P, Signori F, Lazzeri A, et al. Monomers, Materials and Energy from Coffee By-Products: A Review. Sustainability. 2021;13(12):6921.
13. Gonçalves B, Camillo M, Oliveira M, Carreira L, Moulin J, Fantuzzi Neto H, et al. Surface Treatments of Coffee Husk Fiber Waste for Effective Incorporation into Polymer Biocomposites. Polymers. 2021;13(19):3428.
14. Optical and Chemical Investigations of PEO Thin Films Incorporated with Curcumin Nanoparticle: Effect of Film Thickness. Biointerface Research in Applied Chemistry. 2022;13(2):143.
15. Abdali K, Abass KH, Al-Bermany E, Al-robayi EM, Kadim AM. Morphological, Optical, Electrical Characterizations and Anti- Escherichia coli Bacterial Efficiency (AECBE) of PVA/PAAm/PEO Polymer Blend Doped with Silver NPs. Nano Biomed Eng. 2022;14(2).
16. Alhagri IA, Qahtan TF, Farea MO, Al-Hakimi AN, Al-Hazmy SM, Saeed SE-S, et al. Enhanced Structural, Optical Properties and Antibacterial Activity of PEO/CMC Doped TiO_2 NPs for Food Packaging Applications. Polymers. 2023;15(2):384.
17. Muheddin DQ, Aziz SB, Mohammed PA. Variation in the Optical Properties of PEO-Based Composites via a Green Metal Complex: Macroscopic Measurements to Explain Microscopic Quantum Transport from the Valence Band to the Conduction Band. Polymers. 2023;15(3):771.
18. Kim M, Lee L, Jung Y, Kim S. Study on Ion Conductivity and Crystallinity of Composite Polymer Electrolytes Based on Poly(ethylene oxide)/Poly(acrylonitrile) Containing Nano-Sized Al_2O_3 Fillers. Journal of Nanoscience and Nanotechnology. 2013;13(12):7865-7869.
19. Yang Z, Zhang Y, Wen B. Enhanced electromagnetic interference shielding capability in bamboo fiber@ polyaniline composites through microwave reflection cavity design. Composites Science and Technology. 2019;178:41-49.
20. Soori S, Eslahi N, Jahanmardi R. Preparation and Characterization of Self-Healing Nanocomposite Hydrogels Based on Chitosan/Polyethylene Glycol/Bacterial Nanocellulose for Biomedical Applications. Elsevier BV; 2025.
21. Gondaliya N, Kanchan DK, Sharma P, Joge P. Structural and Conductivity Studies of Poly(Ethylene Oxide) – Silver Triflate Polymer Electrolyte System. Materials Sciences and Applications. 2011;02(11):1639-1643.
22. Čović A, Stipanelov Vrandečić N. Influence of poly(ethylene oxide) sample preparation on the results of thermogravimetric analysis. St open. 2021;2:1-13.
23. Ahmed HT, Abdullah OG. Preparation and Composition Optimization of PEO:MC Polymer Blend Films to Enhance Electrical Conductivity. Polymers. 2019;11(5):853.
24. Solaberrieta I, Jiménez A, Cacciotti I, Garrigós MC. Encapsulation of Bioactive Compounds from Aloe Vera Agrowastes in Electrospun Poly (Ethylene Oxide) Nanofibers. Polymers. 2020;12(6):1323.
25. Goldstein JI, Newbury DE, Echlin P, Joy DC, Lyman CE, Lifshin E, et al. Special Topics in Scanning Electron Microscopy. Scanning Electron Microscopy and X-ray Microanalysis: Springer US; 2003. p. 195-270.
26. Di Marco G. Solid state electrochromic device: behaviour of different salts on its performance. Solid State Ionics. 2000;127(1-2):23-29.
27. Jaramillo LY, Vásquez-Rendón M, Upegui S, Posada JC, Romero-Sáez M. Polyethylene-coffee husk eco-composites for production of value-added consumer products. Sustainable Environment Research. 2021;31(1).
28. Abdelghany AM, Abdelrazek EM, Badr SI, Morsi MA. Effect of gamma-irradiation on (PEO/PVP)/Au nanocomposite: Materials for electrochemical and optical applications. Materials and Design. 2016;97:532-543.
29. Hashim FS, Jabbar SA, Al-Bermany E, Abdali K. Effect of Inclusion ZnO-Co_3O_4 Nanoparticles on the Microstructural and Optical Properties of PVA-CMC Polymeric Blend for Biomedical, UV Shielding, and Nuclear Radiation Shielding Applications. Plasmonics. 2024.
30. Hassan AAM, Al-Ogaili AOM. The Impact of Psyllium Husk Addition on the Some Physical Properties of PEO Polymer. Revue des composites et des matériaux avancés. 2025;35(1):71-79.
31. Banerjee M, Jain A, Mukherjee GS. Spectroscopic Evaluation of Optical Parameters of a Transition Metal Salt Filled Polymer Material. Def Sci J. 2018;68(2):225.
32. Hassouni MH, Mishjil KA, Chiad SS, Habubi NF. Effect of Gamma Irradiation on the Optical Properties of Mg Doped CdO Thin Films Deposited by Spray Pyrolysis. International Letters of Chemistry, Physics and Astronomy. 2013;16:26-37.
33. Jabbar SA, Khalil SM, Abdulridha AR, Al-Bermany E, Karar A. Dielectric, AC Conductivity and Optical Characterizations of (PVA-PEG) Doped SrO Hybrid Nanocomposites. Key Eng Mater. 2022;936:83-92.
34. Liu Y. Characterization of structural and optical properties of Zinc Oxide thin films: Nanyang Technological University.
35. Abdali K, Al-Bermany E, Abass KH. Impact the silver nanoparticles on properties of new fabricated polyvinyl alcohol- polyacrylamide- polyacrylic acid nanocomposites films for optoelectronics and radiation pollution applications. Journal of Polymer Research. 2023;30(4).
36. Al-Rubaye SAJ, A. Al-lsawi N, Abdulridha AR. Preparation and Study the Electrical and Optical Properties for (PVA-PEG-Sr_2O_3) Nanocomposites. Neuroquantology. 2021;19(10):47-55.